## Large-Pore Mesoporous Materials with Semi-Crystalline Zeolitic Frameworks**

Do Trong On and Serge Kaliaguine*

Mesoporous molecular sieves with well-defined pore diameters of 20–500 Å[1–3] overcome the pore diameter constraint of zeolites ($<10$ Å)[4] and allow the diffusion of larger molecules. Furthermore, high surface area and tunable pore size are among the many desirable properties that have made such materials the focus of great interest. However, these materials do not show short-range order and, from this point of view, are closer to amorphous than zeolitic materials. As a consequence, the mesoporous silica–alumina have sites that are less acidic than those of zeolites, and do not exhibit the spectacular catalytic properties of acidic zeolites. Moreover, their hydrothermal stability is low and their industrial use as catalysts is rather limited to date.[1–3, 5, 6] Therefore, to upgrade the performances of mesoporous molecular sieves and zeolites, attempts have been made to synthesize a new type of material, which would combine the advantages of these two kinds of molecular sieves. To date, only a few articles concerning this study have been published.[7–12] For example, Kloetstra et al.[7] prepared MCM-41/FAU composites which gave a clear improvement in catalytic activity in the cracking of vacuum gasoil. Huang et al.[9] reported the synthesis of an MCM-41/ZSM-5 composite containing an interconnected mesopore and micropore structure. Attempts to crystallize the mesopore walls of mesostructured materials resulted in the formation of materials with increased thermal stability and catalytic activity.[10–14] A synthesis of a partially crystalline bimodal pore system with combined micro- and mesopores, for example, ITQ, has been achieved by delaminating the layered zeolite MCM-22 and ferrierite (FER).[10] Entrapped unit cells of ZSM5 contained in Al-MCM-41 and Al-HMS were prepared by ion exchange of the mesoporous aluminosilicates with tetrapropylammonium cation (TPA+) as an MFI-structure directing agent and then digestion of the mesoporous materials in glycerol at 120 °C.[11] Pinnavaia and

co-workers[12, 17] and Zhang et al.[18] recently reported steam-stable aluminosilicate mesostructures assembled from zeolite-type seeds such as zeolite Y, ZSM-5, and zeolite beta. In the latter cases, the X-ray diffraction (XRD) patterns did not show crystalline features. Evidence for the presence of zeolite units cells may however be provided by the acid catalytic activity of such materials toward cumene cracking.[11, 12]

Herein, we describe a new general method for the production of a new type of material with semi-crystalline zeolitic mesopore walls. This procedure involves a templated solid-state secondary crystallization of zeolites starting from the amorphous mesoporous materials of corresponding elemental composition. It is important that the walls of the amorphous mesoporous precursor material are as thick as possible. References [2, 3] provide methods for the preparation of mesoporous precursors that are useful in this context including the synthesis and characterization of the mesoporous materials with semi-crystalline ZSM-5 walls by the use of poly(alkylene oxide) triblock copolymer $HO(CH_2CH_2O)_{20}(CH_2CH(CH_3)O)_{70}(CH_2CH_2O)_{20}H$ (designated as $EO_{20}PO_{70}EO_{20}$ or Pluronic P-123, BASF) and tetrapropylammonium hydroxide (TPAOH) as the surfactant and zeolite template, respectively.

Table 1 summarizes the physico-chemical properties of the series of samples obtained after different lengths of crystallization time and designated as [x]UL-ZSM-5, where $x$ is crystallization time in days ($x=0$ is the sample before crystallization). The zeolite ZSM-5 was used as a reference. Reliable information about the effect of crystallization conditions on the mesopore structure as well as the crystalline phase has been obtained from nitrogen adsorption experiments, transmission electron micrograph (TEM) images, and from XRD patterns.

The nitrogen adsorption/desorption isotherm from the calcined [2]UL-ZSM-5 sample after 2 days of crystallization at 130 °C, exhibits typical type IV adsorption/desorption isotherm shape with a $H_1$ hysteresis loop and steep rises at low relative $P/P_0$ pressure indicating the presence of both mesopore and micropore structures (Figure 1). The micro-

Table 1. Physico-chemical properties of UL-ZSM-5[a] and ZSM-5.[b]

| Material | $S_{BET}$ [m²g⁻¹] | $S_{BJH}$ [m²g⁻¹] | $S_{micropore}$ [m²g⁻¹] | Micropore volume [cm³g⁻¹] | Mesopore volume [cm³g⁻¹] | Mesopore diameter [Å] | Crystallinity [%] |
|---|---|---|---|---|---|---|---|
| [0]UL-ZSM-5 | 865 | 745 | 120 | 0.020 | 1.25 | 56 | – |
| [1]UL-ZSM-5 | 825 | 560 | 265 | 0.100 | 1.83 | 118 | ca. 3 |
| [2]UL-ZSM-5 | 645 | 275 | 370 | 0.145 | 1.86 | 205 | 14 |
| [5]UL-ZSM-5 | 565 | 130 | 435 | 0.158 | 1.25 | 290 | 42 |
| ZSM-5 | 490 | 35 | 465 | 0.195 | – | – | 100 |

[a] [x]UL-ZSM-5 where $x$ = crystallization time in days (atomic Si/Al = 100/1). [b] ZSM-5 (atomic Si/Al = 57/1).

[*] Dr. D. Trong On, Prof. S. Kaliaguine
Department of Chemical Engineering
Laval University
Quebec G1K 7P4 (Canada)
Fax: (+) 418-656-3810
E-mail: kaliagui@gch.ulaval.ca

pore and mesopore size distribution (MMSD) was calculated using Horváth–Kawazoe (HK) and Barrett–Joyner–Halenda (BJH) methods, respectively (Figure 1 insert) which show a narrow pore-size distribution of both micropores and mesopores with an average pore diameter of 5.7 and 205 Å, respectively. With increasing crystallization time, the samples exhibit nitrogen adsorption/desorption isotherms with similar inflection but a shift toward higher $P/P_0$ values over a larger
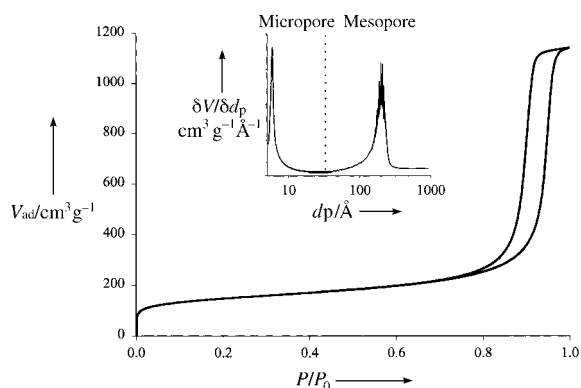
Figure 1. Adsorption/desorption isotherms of nitrogen at $-196\,^{\circ}$C on the calcined [2]UL-ZSM-5 sample. Insert: HK micropore and BJH mesopore size distributions. $d_p$ = pore diameter.

$P/P_0$ range. A significant increase in the pore diameter and a broader pore-size distribution were observed with increasing crystallization time, while the micropore volume increased from 0.020 to 0.158 cm$^3$g$^{-1}$ with no essential change in the micropore diameter (ca. 5.7 Å). The evolution of the MMSD is shown in Figure 2. The micropore diameter of ca. 5.7 Å is comparable to the value known for the crystallographic aperture of the 10-membered-ring zeolite ZSM-5. Note that for highly crystalline ZSM-5, the micropore volume is approximately 0.20 cm$^3$g$^{-1}$ (see Figure 2e and Table 1). The increase in micropore volume suggests that nanoparticles of this zeolite have grown within the mesopore walls. Further-
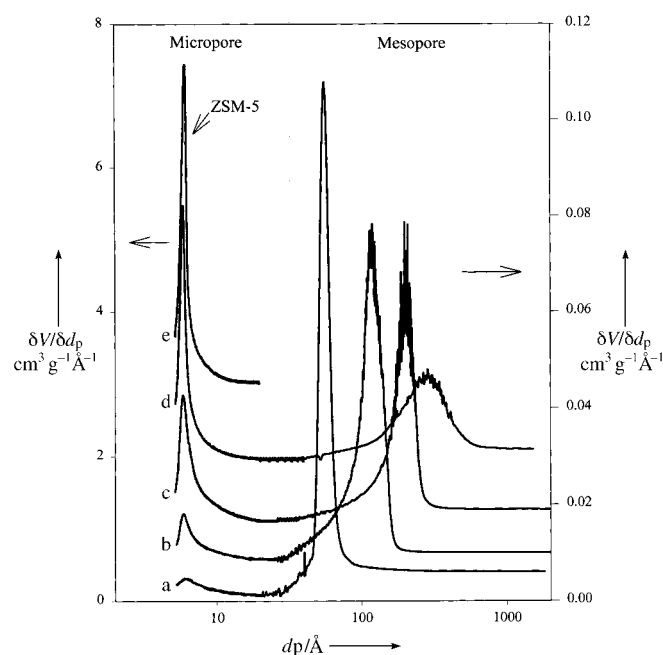


Figure 2. HK micropore and BJH mesopore size distributions for ZSM-5 and the [x]UL-ZSM-5 samples at different lengths of crystallization time: a) before crystallization, b) 1 day, c) 2 days, d) 5 days, and e) ZSM-5.

more, as the crystallization time is increased, the total surface area of the sample ($S_{BET}$; BET = Brunauer–Emmet–Teller) varies from 865 to 565 m$^2$g$^{-1}$ and the mesopore surface area ($S_{BJH}$) varies from 745 to 130 m$^2$g$^{-1}$. Concomitantly, the

micropore surface area ($S_{micropore}$) increases from 120 to 435 m$^2$g$^{-1}$ for this series of samples (Table 1). This indicates some modification of the tubular channels of these materials during crystallization.

The crystalline phase in [x]UL-ZSM-5 upon crystallization was characterized by wide-angle XRD diffractograms, as shown in Figure 3. The mesoporous precursor with amorphous walls (Figure 3a) provides a starting material from
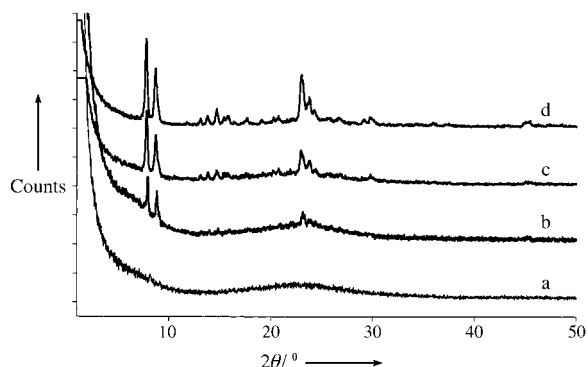


Figure 3. XRD patterns of the calcined [x]UL-ZSM-5 samples after different lengths of crystallization time: a) before crystallization, b) 1 day, c) 2 days, and d) 5 days.

which nano-crystalline domains can nucleate within the walls. The XRD diffractogram of the calcined sample in Figure 3b shows broad peaks, which match those of ZSM-5. These peaks grow in intensity as the crystallization time is increased (Figure 3c, d). By considering ZSM-5 as being 100% crystalline, the crystallinity of the samples was determined (Table 1). About 42% crystallinity was reached after 5 days of crystallization at 130°C. These data indicate that the initially amorphous walls of the mesoporous material are progressively transformed into crystalline nanoparticles. Furthermore, the [5]UL-ZSM-5 sample shows an FT-infrared (IR) absorption band at 561/547 cm$^{-1}$ (doublet) which is not present in the mesoporous precursor (the FT-IR spectra are not shown). This band around 550 cm$^{-1}$ has been assigned to the asymmetric stretching mode in five-membered ring blocks; the splitting of this lattice-sensitive band into a doublet at 561/547 cm$^{-1}$ is characteristic of nanocrystals of the MFI structure (ZSM-5).[13]

A TEM image of the precursor sample before crystallization is shown in Figure 4 and exhibits a uniform pore size with a highly disordered pore structure. This is reminiscent of MSU-1[14] and KIT-1,[15] which have wormhole-type pore structures. Figures 5A and 5B show bright- and dark-field TEM images recorded on the same area of [5]UL-ZSM-5, the bright spots in the image correspond to ZSM-5 nanocrystals. The nanocrystals are embedded in the continuous amorphous inorganic matrix to form semicrystalline wall structures while preserving the mesoporous structure. The wormhole pore lattice is however still present and micro-domains of the order of 10–30 nm are observed. This indicates that the pore walls consist of nanocrystals of this zeolite. However, some agglomerates of segregated zeolite crystals, as seen from the dark field images, indicate that the synthesis procedure could
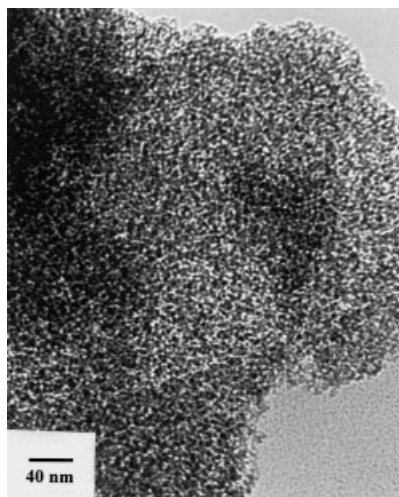
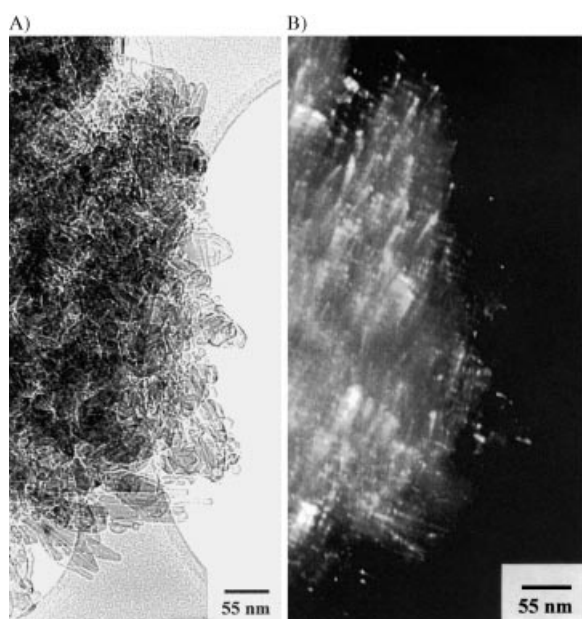Figure 4. TEM image of the calcined [0]UL-ZSM-5 sample.



Figure 5. Bright-field (A) and dark-field (B) TEM images of the same area of the [5]UL-ZSM-5 sample.

still be optimized to generate products containing uniform nanocrystals within the mesopore walls. The $^{27}$Al MAS NMR spectra of the samples exhibit a single resonance centered at $\delta = 54 - 58$, which is characteristic of tetrahedral aluminum. To determine the acidity, pyridine adsorption/desorption experiments were performed. The IR spectra of the pyridine adsorbed on the samples before and after crystallization for 5 days, and of ZSM-5 (atomic Si/Al = 57/1) as the reference, are shown in Figure 6. For the [0]UL-ZSM-5 sample after evacuation at 150 °C, two very weak IR bands at 1547 cm$^{-1}$ and 1455 cm$^{-1}$, which are characteristic of Brønsted and Lewis-acid sites respectively,[16] are observed. However, the FT-IR spectra of the [5]UL-ZSM-5 and ZSM-5 samples show two intense bands at 1547, 1455 cm$^{-1}$ which were retained even after evacuation at 200 °C, while these bands disappeared in the [0]UL-ZSM-5 sample. This suggests a much stronger acidity in [5]UL-ZSM-5 and ZSM-5 than in [0]UL-

ZSM-5. The order of the acid strength was found to be ZSM-5 > [5]UL-ZSM-5 ≫ [0]UL-ZSM-5 and it opens a new possibility of using this new type of material as acid catalysts.

The highly dispersed amorphous material of a mesoporous molecular sieve as a precursor phase was used to generate unusual mesostructured semizeolitic materials (UL-zeolites) by secondary solid-phase crystallization. The controlled size of the pore walls is taken advantage of, in controlling the crystal size of the zeolite product. For example, in the case of sample [5]UL-ZSM-5, Figure 5B indicates an average nano-particle diameter on the order of 5 nm. This approach is not limited to the use of ZSM-5 type zeolites. In this process, zeolite nanoparticles are grown from the mesopore walls and at the same time the end product retains some of the mesopore surface of the precursor. As a consequence a rather high mesoporous surface is composed of the zeolite particles so that this zeolite surface is accessible to large molecules. It is thus expected that these materials will allow the typical acid reactions catalyzed by ZSM-5 but for large molecules. Actually, such effects are also expected with all UL-zeolites, which should allow catalysis to be extended to larger molecules, not converted in standard zeolites because of spatial restrictions. Moreover, the relatively short diffusion pathways through the thin walls are expected to improve mass transfer and catalytic reaction efficiency and minimize channel blocking. Detailed studies of the sorption behavior and catalytic properties are currently underway.
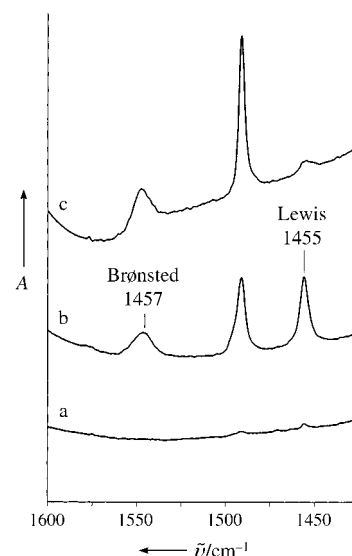


Figure 6. FT-IR spectra of the adsorbed pyridine in the 1350 – 1800 cm$^{-1}$ range after pyridine desorption at 150 °C: a) [0]UL-ZSM-5, b) [5]UL-ZSM-5, and c) ZSM-5.

*Experimental Section*

Synthesis: A series of materials, namely UL-ZSM-5, with atomic ratio Si/Al of 100/1 was prepared using poly(alkylene oxide) triblock copolymer HO(CH$_2$CH$_2$O)$_{20}$(CH$_2$CH(CH$_3$)O)$_{70}$(CH$_2$CH$_2$O)$_{20}$H and tetrapropylam-monium hydroxide as surfactant and zeolite template, respectively. The synthesis of the mesoporous zeolitic materials consists of two steps: 1) preparation of the amorphous mesoporous precursor followed by 2) transformation of the amorphous mesopore walls into crystalline walls.

A typical synthesis procedure was as follows: Step 1: An amorphous mesoporous aluminum containing silica (Si/Al = 100/1) was synthesized using $SiCl_4$ and $AlCl_3$ in ethanol, as in ref. [3]. The surfactant-containing mesoporous solid products were recovered and air-dried at room temperature. Step 2: the dried surfactant-containing mesoporous precursor was impregnated with a 10 wt% solution of TPAOH (free from inorganic alkali). The Si/TPAOH ratio was 8/1. After aging at room temperature, the solid was heated at 60 °C to eliminate water, and dried under vacuum for about 24 h at room temperature. Finally, the solid was transferred into a Teflon-lined autoclave and heated at 130 °C for different lengths of time. It is considered that the quantity of water adsorbed on the solid plays an important role in the crystallization process. Therefore, the partly crystalline solid was further crystallized at the same temperature for a given time after introducing a small amount of water. Because the solid-state crystallization continues in the presence of this small amount of water, the above process permits control of the crystallinity and the mesopore size of the solid materials. The products were washed with distilled water, dried in air at 80 °C, and finally calcined at 550 °C for 6 h to remove the organics.

Characterization: Powder XRD patterns of the materials were recorded on a Philips X-ray diffractometer (PW 1010 generator and PW 1050 computer-assisted goniometer) using nickel-filtered $Cu_{K\alpha}$ ($\lambda = 1.5406$ Å) radiation, 0.025° step size and a 1 s step time. Nitrogen adsorption and desorption isotherms at $-196$ °C were established using an Omnisorp-100 apparatus. The specific surface area ($S_{BET}$) was determined from the linear part of the BET equation ($P/P_0 = 0.05 - 0.15$). The micropore size distribution was calculated from argon adsorption isotherms with the Horváth–Kawazoe method. The calculation of the mesopore-size distribution was performed using the desorption branch of the $N_2$ adsorption/desorption isotherms and the BJH formula. The mesopore surface area ($S_{BJH}$) and mesopore volume ($V_{BJH}$) were obtained from the pore-size distribution curves. The average mesopore diameter, $d_p$, was calculated as $4V_{BJH}/S_{BJH}$. Although its accuracy is limited, the BJH method, which is still universally utilized in the mesoporous molecular sieves (MMS) literature yields results that are comparable with the current literature values. High-resolution TEM images were obtained on a JEOL 200 CX transmission electron microscope operated at 120 kV. The samples for TEM were prepared by dispersing the fine powders of the products in a slurry in ethanol onto honeycomb carbon copper grids. Solid-state $^{27}Al$ and $^{29}Si$ MAS NMR spectra were recorded at room temperature on a Bruker ASX 300 spectrometer.

[1] a) C. T. Kresge, M. E. Leonowicz, W. J. Roth, J. C. Vartuli, J. S. Beck, *Nature* **1992**, *359*, 710–712; b) J. S. Beck, J. C. Vartuli, W. J. Roth, M. E. Leonowicz, C. T. Kresge, K. D. Schmitt, C. T.-W. Chu, D. H. Olsen, E. W. Sheppard, S. B. McCullen, J. B. Higgins, J. L. Schlenker, *J. Am. Chem. Soc.* **1992**, *114*, 10834–10843.

[2] a) D. Zhao, J. Feng, Q. Huo, N. Melosh, G. H. Fredrickson, B. F. Chmelka, G. D. Stucky, *Science* **1998**, *279*, 548–552; b) D. Zhao, Q. Huo, J. Feng, B. F. Chmelka, G. D. Stucky, *J. Am. Chem. Soc.* **1998**, *120*, 6024.

[3] P. Yang, D. Zhao, D. I. Margolese, B. F. Chmelka, G. D. Stucky, *Nature* **1998**, *396*, 152.

[4] A. Corma, *Chem. Rev.* **1995**, *95*, 559.

[5] a) D. Trong On, P. N. Joshi, S. Kaliaguine, *J. Phys. Chem.* **1996**, *100*, 6743; b) E. Dumitriu, D. Trong On, S. Kaliaguine, *J. Catal.* **1997**, *170*, 150.

[6] a) D. Trong On, S. M. J. Zaidi, S. Kaliaguine, *Microporous Mesoporous Mater.* **1998**, *22*, 211; b) D. Trong On, M. P. Kapoor, P. N. Joshi, L. Bonneviot, S. Kaliaguine, *Catal. Lett.* **1997**, *44*, 171.

[7] K. R. Kloetstra, H. W. Zandbergen, J. C. Jansen, H. van Bekkum, *Microporous Mater.* **1996**, *6*, 287.

[8] A. Karlsson, M. Stocker, R. Schmidt, *Microporous Mesoporous Mater.* **1999**, *27*, 181.

[9] L. Huang, W. Guo, P. Deng, Z. Xue, Q. Li, *J. Phys. Chem. B* **2000**, *104*, 2817.

[10] a) A. Corma, V. Fornes, S. B. Pergher, T. L. M. Maesen, J. G. Buglass, *Nature* **1998**, *396*, 353; b) A. Corma, U. Diaz, M. E. Domine, V. Fornes, *J. Am. Chem. Soc.* **2000**, *122*, 2804.

[11] K. R. Kloetstra, H. van Bekkum, J. C. Jansen, *Chem. Commun.* **1997**, 2281.

[12] Y. Liu, W. Zhang, T. J. Pinnavaia, *J. Am. Chem. Soc.* **2000**, *122*, 8791.

[13] R. Ravishankar, C. Kirschhock, B. J. Schoeman, P. Vanoppen, P. J. Grobet, S. Storck, W. F. Maier, J. A. Martens, F. C. De Schryver, P. A. Jacobs, *J. Phys. Chem. B* **1998**, *102*, 2633.

[14] S. A. Bagshaw, E. Prouzet, T. J. Pinnavaia, *Science* **1995**, *269*, 1242.

[15] R. Ryoo, J. M. Kim, C. H. Ko, C. H. Shin, *J. Phys. Chem.* **1996**, *100*, 17718.

[16] R. Borade, A. Sayari, A. Adnot, S. Kaliaguine, *J. Phys. Chem.* **1990**, *94*, 5989.

[17] Y. Liu, W. Zhang, T. J. Pinnavaia, *Angew. Chem.* **2001**, *113*, 1295; *Angew. Chem. Int. Ed.* **2001**, *40*, 1255.

[18] Z. Zhang, Y. Han, L. Zhu, R. Wang, Y. Yu, S. Qiu, D. Zhao, F.-S. Xiao, *Angew. Chem.* **2001**, *113*, 1298; *Angew. Chem. Int. Ed.* **2001**, *40*, 1258.

# A Redox Switch Based on Dihydro[5]helicene: Drastic Chiroptical Response Induced by Reversible C−C Bond Making/Breaking upon Electron Transfer**

Jun-ichi Nishida, Takanori Suzuki,* Masakazu Ohkita, and Takashi Tsuji

Helicenes are a special series of chiral molecules with huge optical activities, and thus attract considerable attention for use as nonlinear optical (NLO) materials and asymmetric catalysts.[1] Chiroptical photoswitches that function by modulating the helical geometries of helicenes by light have also been constructed.[2] However, the electron-transfer (ET) reaction of chiral helicenes has not been reported although they can serve as novel "electrochiroptical" transducers when redox-active groups are incorporated. We have found that dihydro[5]helicenes **1** which contain two electron-donating spiro rings undergo reversible C−C bond breaking to give

[*] Prof. Dr. T. Suzuki, Dr. J. Nishida,[+] Dr. M. Ohkita, Prof. Dr. T. Tsuji
Division of Chemistry
Graduate School of Science
Hokkaido University, Sapporo 060-0810 (Japan)
Fax: (+81) 11-746-2557
E-mail: tak@sci.hokudai.ac.jp

[+] Present address:
Department of Electronic Chemistry, Interdisciplinary School of Science and Engineering, Tokyo Institute of Technology
Yokohama 226-8502 (Japan)

Supporting information for this article is available on the WWW under http://www.angewandte.com or from the author.